Available online at www.sciencedirect.com
ScienceDirect
Journal of Sound and Vibration 301 (2007) 146–164
JOURNAL OF SOUND AND VIBRATION
www.elsevier.com/locate/jsvi

Dynamic modeling and performance evaluation of a vibrating beam microgyroscope under general support motion

Mehdi Esmaeili[a], Nader Jalili[b,*], Mohammad Durali[a]

[a]*Mechanical Engineering Department, Sharif University of Technology, P.O. Box 11365-9567, Tehran, Iran*
[b]*Smart Structures and Nanoelectromechanical Systems Laboratory, Department of Mechanical Engineering, Clemson University, Clemson, SC 29634-0921, USA*

Received 15 August 2005; received in revised form 18 September 2006; accepted 19 September 2006
Available online 17 November 2006

Abstract

A general modeling framework is presented for the development of the frequency equation of a microgyroscope, which is modeled as a suspended cantilever beam with a tip mass under general base excitation. Specifically, the beam is considered to vibrate in all the three directions, while subjected to a base rotational motion around its longitudinal direction. This is a common configuration utilized in many vibrating beam gyroscopes and well drilling systems. The governing equations are derived by using the Extended Hamilton's Principle with a general 6-dof base motion. The natural frequency equation is then extracted in a closed-form for the case where the beam support undergoes longitudinal rotation. The effect of substrate motions on the performance of microgyroscopes is also discussed, along with the effects of a beam-distributed mass, a tip mass, angular accelerations, centripetal accelerations and Coriolis accelerations. The response of the system to different inputs is studied and the response sensitivity to input parameter variations is examined. Finally, the sources of error in the measurement of input rotational speed are investigated and identified. The results of the study demonstrate the importance of errors, caused by cross axes inputs, on the gyroscope output measurements.

1. Introduction

Many research studies have been concentrated on the vibrations of flexible beams with different boundary conditions and engineering applications. One of the typical models consists of a uniform flexible cantilever beam carrying a tip mass. Antennas, rotating blades, deep well drills, and vibrating beam microgyroscopes serve as engineering applications of such model. Among the research studies focused on developing models for the analysis of this problem, the following can be mentioned. Bhat and Wagner [1] carried out a detailed analysis to develop the frequency equations for a cantilever beam with tip mass. Anderson [2] developed a beam model with asymmetric tip mass. Parnell and Cobble [3] solved the equations of a cantilever beam with end mass for different boundary conditions and lateral forces using Laplace transformation. Laura et al. [4] derived the frequency equations of a clamped–free beam with a finite mass at the free end, and Gürgöze [5] performed similar work for the case in which a mass-spring system was attached to the tip mass. Most of the models developed are for cases

*Corresponding author. Tel.: +864 656 5642; fax: +864 656 4435.
E-mail address: Jalili@clemson.edu (N. Jalili).

0022-460X/$ - see front matter © 2006 Elsevier Ltd. All rights reserved.
doi:10.1016/j.jsv.2006.09.026

in which the beam support is stationary. The first modeling work based on the classical linear Cartesian method was done in early 1970s [6,7]. In the analysis of these models, finite element methods with linear beam properties were utilized. Later works adopted this method and applied it to a wide range of engineering problems.

Recent advancements in microtechnology have brought about new possibilities for manufacturing microgyroscopes. These devices are many times smaller than their macroscopic counterparts. Development of microgyroscopes and MicroElectroMechanical Systems (MEMS) has generated new markets and opportunities in low cost–medium performance of inertial systems such as useable electronic systems, automobile applications, Global Positioning Systems, and even more recently in a wide range of military applications. Naturally, a great deal of effort is put forth into improving their performance and increasing their range of applications [8,9]. A large portion of these efforts is concentrated on solving production problems and eliminating undesirable results of micromachining [10–12].

Among different types of microgyroscopes, suspended vibrating ones consisting of rings, vibrating beams and tuning forks are the most commonly used configurations of gyroscopes. The main reason behind this is the compatibilities of their batch production procedures with today's technology. The main part of a microgyroscope is a cantilever supporting a mass at the end [13,14]. Increasing the tip mass will affect gyroscope's performance by increasing the effect of rotation rate, increasing the gyroscopic effects and reducing the effects of undesirable Brownian noise. Microgyroscopes with a vibrating beam work because of the Coriolis acceleration induced by the input rotation rate. If the beam has lateral (bending) oscillations, any input rotation along its longitudinal axis will induce oscillations due to Coriolis effects in the lateral direction normal to the input oscillations. By measuring the induced oscillation, for instance by using capacitive or piezoelectric sensors, the input rotation rate can be measured. If the beam rotation is around the longitudinal axis only, the measurements will be accurate. In practice, however, the device can have other rotations too, which will alter the measurements. In fact, one of the major sources of error in microgyroscope performance is caused by the rotations of the substrate.

One of the main objectives of the current research described here is to develop a model for the analysis of a cantilever beam with a tip mass under general support motions. The current work is motivated by the fact that such a system is extensively used in vibrating beam gyroscopes and well drilling systems. Hence, such model development may provide additional design information for better performance evaluation. Generally, a gyroscope can be considered as a sensor used for measurement of rotational speed, used in a wide range of industrial applications in navigation and control of aerial and ground vehicles.

The second objective of this research is to study the effects of different combinations of substrate motions on the performance of the vibrating cantilever beam microgyroscope. To perform this, a beam model is constructed and its lateral amplitudes in two directions are estimated by using the assumed mode model (AMM) expansion as a linear combination of generalized coordinates. By using Hamilton's principle, the system's governing equations are derived. By solving these equations, the effects of undesirable rotations and motions other than input rotation on the system response can be studied. By recognizing the effects of input disturbances on system performance, proper elimination strategies can be devised to improve microgyroscope performance.

2. Governing equations of motion in general form

To obtain the governing equations of motion of a cantilever beam with a tip mass, the Extended Hamilton's Principle is utilized here. The beam is considered to obey the Euler–Bernoulli beam theory with small thickness to length ratio. In addition, the torsional vibration effects are ignored. To express the potential and kinetic energies, three Cartesian variables u_i, $i = 1$, 2 and 3, measured in moving coordinate system, are used. Fig. 1 depicts the beam with a concentrated mass at its free end, which is subjected to a support motion in coordinate system $\{\mathbf{a}_i\}$.

As a result of base motion, point P^* on the neutral axis of beam is moved to point P. The position and velocity of point P in the reference frame $\{\mathbf{A}_i\}$ can be expressed as

$$\begin{aligned}
\mathbf{r}_P &= \mathbf{u}_{P^*} + \mathbf{r}_{P^*} + \mathbf{r}_{O'},\\
\dot{\mathbf{r}}_P &= \dot{\mathbf{r}}_{O'} + \frac{\partial \mathbf{u}_{P^*}}{\partial t} + \boldsymbol{\omega}_{\text{sub}} \times (\mathbf{u}_{P^*} + \mathbf{r}_{P^*}),\\
\dot{\mathbf{r}}_P &= V_i \mathbf{a}_i + \frac{\partial u_i}{\partial t}\mathbf{a}_i + \omega_j \mathbf{a}_j \times (u_i \mathbf{a}_i + x\mathbf{a}_1),
\end{aligned} \tag{1}$$

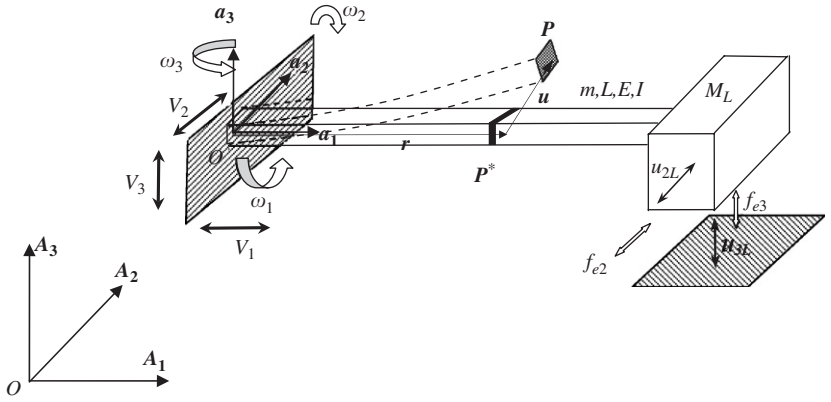

Fig. 1. The schematic of the cantilever beam with tip mass under general base motion.

with the variables as defined in Fig. 1. In these equations, $\boldsymbol{\omega}_{\text{sub}}$ (which is equal to $\omega_i \mathbf{a}_i$) is the rotation of the base relative to the reference frame, and x is the position of point P in the moving coordinate system. Simplifying the vector products used in Eq. (1), the velocities of point P can be reduced to

$$\begin{aligned}
&\dot{\mathbf{r}}_P = h_i \mathbf{a}_i,\\
&h_1 = V_1 + \frac{\partial u_1}{\partial t} + u_3\omega_2 - u_2\omega_3,\\
&h_2 = V_2 + \frac{\partial u_2}{\partial t} + u_1\omega_3 - u_3\omega_1 + x\omega_3,\\
&h_3 = V_3 + \frac{\partial u_3}{\partial t} + u_2\omega_1 - u_1\omega_2 - x\omega_2,
\end{aligned} \tag{2}$$

where $\mathbf{a}_i$ represents the ith unit vector.

Consequently, the total kinetic energy of the beam incorporating both tip and beam distributed masses can be expressed as

$$T = \frac{1}{2}\int_0^L mT^*(x, u_i, V_i, \omega_i)\,\mathrm{d}x + \frac{1}{2}M_L T^*(L, u_{i_{x=L}}, V_i, \omega_i), \tag{3}$$

$$T^*(x, u_i, V_i, \omega_i) = h_1^2 + h_2^2 + h_3^2, \tag{4}$$

where m is the beam mass per unit length, and M_L represents the tip mass. The beam strain (potential) energy can also be written as

$$V = \frac{1}{2}\int_0^L EA\left(\frac{\partial u_1}{\partial x}\right)^2 \mathrm{d}x + \frac{1}{2}\int_0^L EI_{33}\left(\frac{\partial^2 u_2}{\partial^2 x}\right)^2 \mathrm{d}x + \frac{1}{2}\int_0^L EI_{22}\left(\frac{\partial^2 u_3}{\partial^2 x}\right)^2 \mathrm{d}x, \tag{5}$$

where L is the beam length. Using the Extended Hamilton's Principle, the equations of motion of the beam can be extracted as detailed in Appendix A and summarized here:

$$\begin{aligned}
&m\left[-\frac{\partial h_1}{\partial t} + h_2\omega_3 - h_3\omega_2\right] + \frac{\partial}{\partial x}\left(EA\frac{\partial u_1}{\partial x}\right) = 0,\\
&m\left[-\frac{\partial h_2}{\partial t} + h_3\omega_1 - h_1\omega_3\right] - \frac{\partial^2}{\partial x^2}\left(EI_{33}\frac{\partial^2 u_2}{\partial x^2}\right) = 0,\\
&m\left[-\frac{\partial h_3}{\partial t} + h_1\omega_2 - h_2\omega_1\right] - \frac{\partial^2}{\partial x^2}\left(EI_{22}\frac{\partial^2 u_3}{\partial x^2}\right) = 0,
\end{aligned}$$

$$
\begin{aligned}
&-EA\frac{\partial u_1}{\partial x} - M_L\frac{\partial h_1}{\partial t} + M_L h_2\omega_3 - M_L h_3\omega_2\Big|_{x=L} = 0,\\
&\frac{\partial}{\partial x}\left(EI_{33}\frac{\partial^2 u_2}{\partial x^2}\right) - M_L\frac{\partial h_2}{\partial t} + M_L h_3\omega_1 - M_L h_1\omega_3 + f_{e_2}\Big|_{x=L} = 0,\\
&\frac{\partial}{\partial x}\left(EI_{22}\frac{\partial^2 u_3}{\partial x^2}\right) - M_L\frac{\partial h_3}{\partial t} + M_L h_1\omega_2 - M_L h_2\omega_1 + f_{e_3}\Big|_{x=L} = 0,\\
&EI_{33}\frac{\partial^2 u_2}{\partial x^2}\Big|_{x=L} = 0, \quad EI_{22}\frac{\partial^2 u_3}{\partial x^2}\Big|_{x=L} = 0.
\end{aligned} \tag{6}
$$

3. Closed-form frequency equation for base longitudinal rotation

An example case study is considered here in which the beam undergoes general vibrating motions while subjected only to rotation around its longitudinal axis. This is a common configuration in vibrating beam gyroscopes and deep well drilling systems. In microgyroscopes modeled as vibrating beams with tip mass, the objective is to measure the rotation rate around longitudinal axis. Therefore, it is necessary to extract the frequency equation and natural frequencies of the system in a closed-form, if possible. For this special case, the values of h_1, h_2, and h_3 defined in Eq. (2) reduce to

$$
\begin{aligned}
h_1 &= \frac{\partial u_1}{\partial t},\\
h_2 &= \frac{\partial u_2}{\partial t} - u_3\omega_1,\\
h_3 &= \frac{\partial u_3}{\partial t} + u_2\omega_1.
\end{aligned} \tag{7}
$$

Substituting these expressions into Eq. (6) yields

$$
\begin{aligned}
&-m\frac{\partial^2 u_1}{\partial t^2} + \frac{\partial}{\partial x}\left(EA\frac{\partial u_1}{\partial x}\right) = 0,\\
&-m\frac{\partial^2 u_2}{\partial t^2} + 2m\frac{\partial u_3}{\partial t}\omega_1 + mu_2\omega_1^2 - \frac{\partial^2}{\partial x^2}\left(EI_{33}\frac{\partial^2 u_2}{\partial x^2}\right) = 0,\\
&-m\frac{\partial^2 u_3}{\partial t^2} - 2m\frac{\partial u_2}{\partial t}\omega_1 + mu_3\omega_1^2 - \frac{\partial^2}{\partial x^2}\left(EI_{22}\frac{\partial^2 u_3}{\partial x^2}\right) = 0,\\
&-EA\frac{\partial u_1}{\partial x} - M_L\frac{\partial^2 u_1}{\partial t^2}\Big|_{x=L} = 0,\\
&\frac{\partial}{\partial x}\left(EI_{33}\frac{\partial^2 u_2}{\partial x^2}\right) - M_L\frac{\partial}{\partial t}\left(\frac{\partial u_2}{\partial t} - u_3\omega_1\right) + M_L\left(\frac{\partial u_3}{\partial t} + u_2\omega_1\right)\omega_1\Big|_{x=L} = 0,\\
&\frac{\partial}{\partial x}\left(EI_{22}\frac{\partial^2 u_3}{\partial x^2}\right) - M_L\frac{\partial}{\partial t}\left(\frac{\partial u_3}{\partial t} + u_2\omega_1\right) - M_L\left(\frac{\partial u_2}{\partial t} - u_3\omega_1\right)\omega_1\Big|_{x=L} = 0,\\
&EI_{33}\frac{\partial^2 u_2}{\partial x^2}\Big|_{x=L} = 0,\\
&EI_{22}\frac{\partial^2 u_3}{\partial x^2}\Big|_{x=L} = 0.
\end{aligned} \tag{8}
$$

Furthermore, if the lateral stiffness of the beam in two directions is assumed to be the same and axial strains along the beam can be ignored (when compared with the strains due to bending), the system equations reduce to two equations coupled via gyroscopic terms plus the equations associated

with the boundary conditions:

$$\frac{\partial^4 u_2(x,t)}{\partial x^4} + k_1 \frac{\partial^2 u_2(x,t)}{\partial t^2} - k_2 \frac{\partial u_3(x,t)}{\partial t} = 0,$$
$$\frac{\partial^4 u_3(x,t)}{\partial x^4} + k_1 \frac{\partial^2 u_3(x,t)}{\partial t^2} + k_2 \frac{\partial u_2(x,t)}{\partial t} = 0,$$
$$\frac{\partial^3 u_2(L,t)}{\partial x^3} - rLk_1 \frac{\partial^2 u_2(L,t)}{\partial t^2} + rLk_2 \frac{\partial u_3(L,t)}{\partial t} = 0,$$
$$\frac{\partial^2 u_2(L,t)}{\partial x^2} = 0,$$
$$\frac{\partial^3 u_3(L,t)}{\partial x^3} - rLk_1 \frac{\partial^2 u_3(L,t)}{\partial t^2} - rLk_2 \frac{\partial u_2(L,t)}{\partial t} = 0,$$
$$\frac{\partial^2 u_3(L,t)}{\partial x^2} = 0,$$

where

$$r = \frac{M_L}{mL}, \quad k_1 = \frac{m}{EI} \quad \text{and} \quad k_2 = \frac{2\omega_1 m}{EI}. \tag{9}$$

To obtain the frequency equation, the denominator of the system transfer function is needed, which must not depend on spatial coordinates. However, this operation is affected by the boundary conditions, which depend on spatial coordinates. Hence, both temporal and spatial Laplace transformations are needed to solve this problem. Taking the temporal and spatial Laplace transformations (refer to Appendix B for detailed derivations) will ultimately result in a frequency equation in the form

$$r\beta[\cos(\beta)\sinh(\beta) - \sin(\beta)\cosh(\beta)] + 1 + \cos(\beta)\cosh(\beta) = 0, \tag{10}$$

where $\beta^4 = (-k_1 s^2 \pm k_2 s\mathrm{i})L^4$ and i is the imaginary unit. The general format of this equation is similar to the frequency equation of a cantilever beam with tip mass except for the fact that term $\beta^4 = (-k_1 s^2 \pm k_2 s\mathrm{i})L^4$ is replaced by $\beta^4 = (-k_1 s^2)L^4$, [15–18]. It can therefore be concluded that the fundamental frequencies of a cantilever beam with tip mass, but without rotation along longitudinal axis, can be used for the case in which the beam rotates along its longitudinal axis. This is a valuable conclusion, which could simplify similar analysis. This equation can also be used to determine the natural frequency of beams and shafts that rotate along their longitudinal axis, a situation found in variety of applications such as navigation, microgyroscope and well drills. It seems that this procedure is also applicable for other boundary conditions. Therefore, the need to use numerical solutions for calculating the natural frequencies is omitted. Assume that one of the solutions of Eq. (10) is when of $\beta = \beta_0$, then

$$k_1 s^2 \pm k_2 s\mathrm{i} + \left(\frac{\beta_0}{L}\right)^4 = 0, \quad k_2 = 2\omega_1 k_1 \Rightarrow s = \left(\pm\omega_1 + \sqrt{\frac{\beta_0^4}{k_1 L^4} + \omega_1^2}\right)\mathrm{i}. \tag{11}$$

If β_0 turns out to be real, then s becomes imaginary and we have real frequencies. It can be seen from Eq. (11) that while there is one vibration frequency for the case of a non-rotating beam, there are two frequencies for the case of a beam with rotation. This is in agreement with similar results for rotors with gyroscopic motion as explained next.

4. Comparison of gyroscope results with rigid rotor model

To compare the results obtained from the current analysis, a rotor with a shaft, as depicted in Fig. 2, is taken. It must be noted that the springs in Fig. 2 correspond to the tip stiffness of the shaft and the rotor can be assumed to be rigid. The shaft stiffness and the equivalent moment of inertia for

the rotor are:

$$K = \frac{3EI}{L^3}, \quad I_0 = \left(\frac{mL^3}{3} + M_L L^2\right). \tag{12}$$

The resonance frequencies of this system for a case in which the shaft has equal spring constants in two lateral directions and the rotor is rotating with speed ω_1 can be written as

$$\omega_0 = \pm\omega_1 + \sqrt{\omega_1^2 + \frac{KL^2}{I_0}}. \tag{13}$$

Substituting Eq. (12) into Eq. (13) will yield the equivalent natural frequencies. For a case of a system with the physical properties listed in Table 1, the equivalent frequencies from the rotor model and the fundamental natural frequency of the vibrating beam from Eq. (10) can be compared; these are as shown in Fig. 3.

As seen from Fig. 3, the fundamental natural frequency of the vibrating beam is very close to the rotor frequency. As the base rotational speed increases, the difference between the predictions from the two models reduces. In Fig. 4 is shown the differences between the results of the two models shown in Fig. 3.

Fig. 5 depicts the effect of base rotational speed around the longitudinal axis of the beam on the fundamental mode shape. Reduction in mode shape slope can be seen with increased base rotational speed.

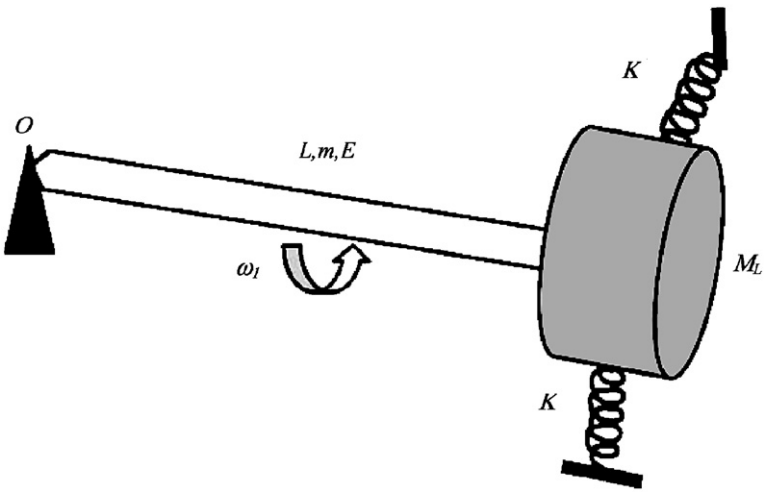

Fig. 2. Schematics of the rotor model.

Table 1
Physical properties of the rotor and beam

Symbol	Description	Numerical values
L	Beam or rotor length (m)	1
ρ	Volumetric density (kg/m^3)	2300
E	Young's modulus of elasticity (N/m^2)	160×10^9
m	Beam or rotor linear density (kg/m)	0.23
M_L	Tip mass (kg)	0.23
I	The beam moment of inertia (m^4)	8.33×10^{-10}

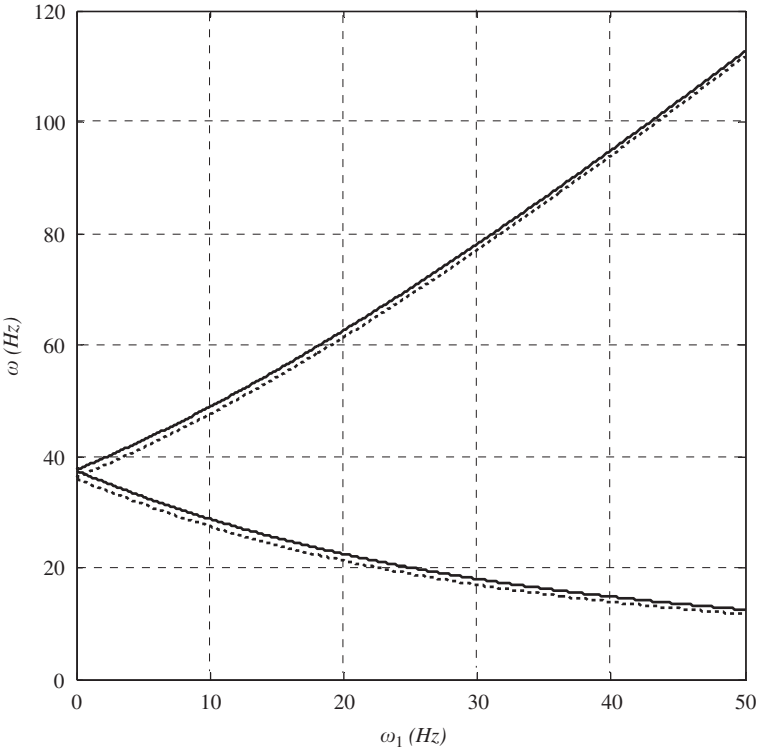

Fig. 3. Fundamental natural frequencies (ω) obtained from the two models as a function of base rotational speed (ω_1). Solid lines (—) results for the rotating beam and dashed lines (- - -) results for the rotor model.

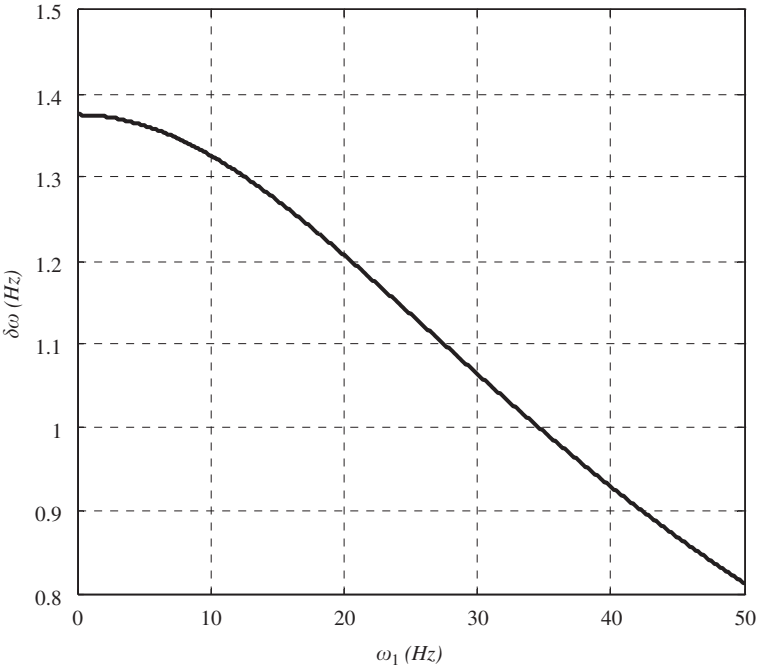

Fig. 4. The differences between the fundamental natural frequencies (ω) of the two models as a function of base rotational speed (ω_1).

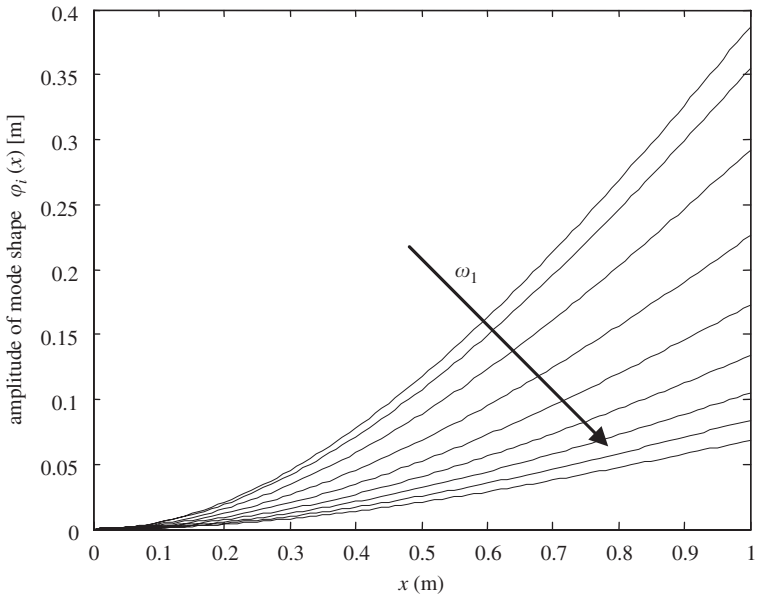

Fig. 5. Effect of the base rotational speed around the longitudinal axis of the beam on the fundamental mode shape.

5. Vibrating beam microgyroscope model

In Fig. 1 is a simple schematic view of a cantilever beam gyroscope. As mentioned earlier, the tip mass and the beam constitute the main elements of the microgyroscope. Any rotation along the longitudinal axis (ω_1), while the beam has lateral oscillations (u_3), will induce oscillations (u_2) in the normal direction. A calibrated measurement of u_2 can lead to determination of ω_1. As indicated in Fig. 1, the beam support can have any possible linear motions or rotations in the frame of reference and this can affect the measurements of ω_1 from u_2. Therefore, a fairly accurate model is required to account for the effects of base motions on system output.

The vibrating beam is treated as an Euler–Bernoulli beam with all the displacements remaining in the elastic zone. The longitudinal strain of the beam is also ignored relative to strains due to lateral motions. Electrostatic forces are used to induce basic lateral oscillations, which are considered here as external effects. To derive the governing equations of motion, the assumed mode model expansion is used as described next.

5.1. Derivation of the governing equations

By using the AMM expansion and ignoring axial strains, displacements u_2 and u_3 are assumed to be linear functions of assumed modes and generalized coordinates. Thus,

$$u_2(x,t)=\sum_{i=1}^{n}\varphi_i(x)q_i(t),\ u_3(x,t)=\sum_{i=1}^{n}\varphi_i(x)p_i(t), \tag{14}$$

where $q_i(t)$ and $p_i(t)$ are generalized coordinates. Substituting Eq. (14) into Eq. (6) will yield the following governing equations:

$$\begin{aligned}
&\mathbf{M}\frac{\mathrm{d}^2\mathbf{x}}{\mathrm{d}t^2}+\mathbf{B}\frac{\mathrm{d}\mathbf{x}}{\mathrm{d}t}+\mathbf{K}\mathbf{x}+\mathbf{T}=\mathbf{F}_S\mathbf{x}+\mathbf{F}_D,\\
&\mathbf{M}=\mathbf{M}_1+\mathbf{M}_2,\\
&\mathbf{B}=\mathbf{B}_1+\mathbf{B}_2,\\
&\mathbf{T}=\mathbf{T}_1+\mathbf{T}_2+\mathbf{R}_1+\mathbf{R}_2,\\
&\mathbf{K}=\mathbf{K}_1+\mathbf{K}_2+\mathbf{K}_3+\mathbf{K}_4+\mathbf{K}_5+\mathbf{K}_6+\mathbf{K}_7+\mathbf{K}_8+\mathbf{K}_9,
\end{aligned} \tag{15}$$

where vector $\mathbf{x}$ is defined as $\mathbf{x} = [\mathbf{q}|\mathbf{p}]^{\mathrm{T}}$ and

$$\mathbf{M}_1 = \begin{bmatrix} \mathbf{M}_d & 0 \\ 0 & \mathbf{M}_d \end{bmatrix}, \quad \mathbf{M}_2 = M_L \begin{bmatrix} \mathbf{F}_1 & 0 \\ 0 & \mathbf{F}_1 \end{bmatrix}, \quad \mathbf{B}_1 = 2\omega_1 \begin{bmatrix} 0 & -\mathbf{M}_d \\ \mathbf{M}_d & 0 \end{bmatrix},$$
$$\mathbf{B}_2 = 2\omega_1 M_L \begin{bmatrix} 0 & -\mathbf{F}_1 \\ \mathbf{F}_1 & 0 \end{bmatrix}, \quad \mathbf{K}_8 = \begin{bmatrix} 0 & (\omega_2\omega_3 - \dot{\omega}_1)\mathbf{M}_d \\ (\omega_2\omega_3 + \dot{\omega}_1)\mathbf{M}_d & 0 \end{bmatrix},$$
$$\mathbf{K}_9 = M_L \begin{bmatrix} 0 & (\omega_2\omega_3 - \dot{\omega}_1)\mathbf{F}_1 \\ (\omega_2\omega_3 + \dot{\omega}_1)\mathbf{F}_1 & 0 \end{bmatrix}, \quad \mathbf{K}_1 = \begin{bmatrix} \mathbf{K}_d & 0 \\ 0 & \mathbf{K}_d \end{bmatrix},$$
$$\mathbf{R}_1 = \begin{bmatrix} (\dot{V}_2 - \omega_1 V_3 + \omega_3 V_1)\mathbf{R} \\ (\dot{V}_3 + \omega_1 V_2 - \omega_2 V_1)\mathbf{R} \end{bmatrix}, \quad \mathbf{R}_2 = M_L \begin{bmatrix} (\dot{V}_2 - \omega_1 V_3 + \omega_3 V_1)\mathbf{F}_L \\ (\dot{V}_3 + \omega_1 V_2 - \omega_2 V_1)\mathbf{F}_L \end{bmatrix}, \quad \mathbf{K}_4 = -\omega_1^2 \mathbf{M}_1,$$
$$\mathbf{K}_5 = -\omega_1^2 \mathbf{M}_2, \quad \mathbf{K}_6 = \begin{bmatrix} -\omega_2^2 \mathbf{M}_d & 0 \\ 0 & -\omega_3^2 \mathbf{M}_d \end{bmatrix}, \quad \mathbf{K}_2 = \dot{\omega}_1 \begin{bmatrix} 0 & -\mathbf{M}_d \\ \mathbf{M}_d & 0 \end{bmatrix},$$
$$\mathbf{K}_7 = M_L \begin{bmatrix} -\omega_2^2 \mathbf{F}_1 & 0 \\ 0 & -\omega_3^2 \mathbf{F}_1 \end{bmatrix}, \quad \mathbf{K}_3 = M_L \dot{\omega}_1 \begin{bmatrix} 0 & -\mathbf{F}_1 \\ \mathbf{F}_1 & 0 \end{bmatrix},$$
$$\mathbf{F}_S = \begin{bmatrix} f_{s2} & \mathbf{F}_L \\ f_{s3} & \mathbf{F}_L \end{bmatrix}, \quad \mathbf{F}_D = \begin{bmatrix} f_{D2}\mathbf{F}_1 & 0 \\ 0 & f_{D3}\mathbf{F}_1 \end{bmatrix}, \quad \mathbf{T}_1 = \begin{bmatrix} (\dot{\omega}_3 + \omega_1\omega_2)\mathbf{T}_F \\ (\dot{\omega}_2 + \omega_1\omega_3)\mathbf{T}_F \end{bmatrix}, \quad \mathbf{R} = [R_1 \dots R_n]^{\mathrm{T}},$$
$$\mathbf{K}_d = \mathrm{diag}(K_{ii}), \quad \mathbf{M}_d = \mathrm{diag}(M_{ii}), \quad \mathbf{F}_1 = \varphi(L)\varphi^{\mathrm{T}}(L), \quad \mathbf{T}_F = [T_{F1} \dots T_{Fn}]^{\mathrm{T}},$$
$$\mathbf{F}_L = \varphi(L), \quad \mathbf{T}_{FM} = M_L L \mathbf{F}_L, \quad \mathbf{T}_2 = \begin{bmatrix} (\dot{\omega}_3 + \omega_1\omega_2)\mathbf{T}_{FM} \\ (\dot{\omega}_2 + \omega_1\omega_3)\mathbf{T}_{FM} \end{bmatrix}, \quad \varphi = [\varphi_1 \dots \varphi_n]^{\mathrm{T}}, \tag{16}$$

$$I_{22} = I_{33} = I, \quad \int_0^L m\varphi_i(x)\varphi_j(x)\,\mathrm{d}x = \delta_{ij} M_{ii},$$
$$\int_0^L EI \frac{\mathrm{d}^2\varphi_i(x)}{\mathrm{d}x^2}\frac{\mathrm{d}^2\varphi_j(x)}{\mathrm{d}x^2}\,\mathrm{d}x = \delta_{ij} K_{ii}, \quad \int_0^L m\varphi_i(x)\,\mathrm{d}x = R_i,$$
$$\int_0^L mx\varphi_i(x)\,\mathrm{d}x = T_{Fi},$$
$$f_{e_2} = f_{S2} + f_{D2} u_{2L}, \quad f_{e_3} = f_{S3} + f_{D3}\, u_{3L}. \tag{17}$$

The definitions of some of the key matrices used in Eqs. (15) and (16) are given in Table 2.

The assumed mode model method is implemented with the properties listed in Table 1, [19,20]. The equations of motion given in Eq. (15) were solved for different combinations of excitation and input conditions. MATLAB was used to perform the calculations. The parameter under study is the measured value and how it changes in each case. Results are summarized in the following subsections. The specifications for the microgyroscope modeled as a beam are listed in Table 3.

5.2. System response to excitation frequency

The excitation frequency has a remarkable effect on the output displacement in the sensing direction. The closer the excitation frequency is to the natural frequency of the beam, the higher the output level will be. This effect is illustrated in Fig. 6 for four different excitation frequencies. In Fig. 6b, the excitation frequency is equal to the natural frequency of the beam. Here, f_{S3}, the electrostatic force in the $\mathbf{a}_3$ direction is $10\sin(\omega_{f_3} t)$ nN, where ω_{f_3} is the frequency of the applied electrostatic force.

Table 2
The definition of matrices used in microgyroscope Eqs. (15) and (16)

Matrices	Description
$\mathbf{M}_1$	The distributed mass (m)
$\mathbf{M}_2$	The end point mass (M_L)
$\mathbf{T}_1$	The effect of m and $\dot{\omega}_2$, $\dot{\omega}_3$, $\omega_1\omega_2$, $\omega_1\omega_3$
$\mathbf{T}_2$	The effect of M_L and $\dot{\omega}_2$, $\dot{\omega}_3$, $\omega_1\omega_2$, $\omega_1\omega_3$
$\mathbf{R}_1$	The effect of m and $\dot{V}_2$, $\dot{V}_3$, $\omega_2 V_1$, $\omega_3 V_1$, $\omega_1 V_2$, $\omega_1 V_3$
$\mathbf{R}_2$	The effect of M_L and $\dot{V}_2$, $\dot{V}_3$, $\omega_2 V_1$, $\omega_3 V_1$, $\omega_1 V_2$, $\omega_1 V_3$
$\mathbf{K}_1$	Stiffness matrix
$\mathbf{K}_2$	The effect of angular acceleration $\dot{\omega}_1$, m
$\mathbf{K}_3$	The effect of angular acceleration $\dot{\omega}_1$, M_L
$\mathbf{K}_4$	The effect of centripetal acceleration m, ω_1
$\mathbf{K}_5$	The effect of centripetal acceleration M_L, ω_1
$\mathbf{K}_6$	The effect of centripetal acceleration m, ω_2, ω_3
$\mathbf{K}_7$	The effect of centripetal acceleration M_L, ω_2, ω_3
$\mathbf{K}_8$	The effect of variable input m, $\dot{\omega}_1$, $\omega_2\omega_3$
$\mathbf{K}_9$	The effect of variable input M_L, $\dot{\omega}_1$, $\omega_2\omega_3$
$\mathbf{B}_1$	The effect of Coriolis and m
$\mathbf{B}_2$	The effect of Coriolis and M_L
$\mathbf{F}_D$	The effect of f_{D2}, f_{D3}
$\mathbf{F}_S$	The effect of f_{S2}, f_{S3}

Table 3
Microgyroscope specifications

Symbol	Description	Numerical values
L	Beam length (μm)	400
ρ	Volumetric density (kg/m^3)	2300
E	Young's modulus of elasticity (N/m^2)	160×10^9
m	Beam linear density (kg/m)	1.803×10^{-8}
M_L	Tip mass (kg)	7.2128×10^{-12}
I	Moment of inertia (m^4)	5.1221×10^{-24}

5.3. System response to excitation amplitude

In Fig. 7 the system response to four different excitation force amplitudes, all at excitation frequency of $\omega_1 = 20$ rad/s, are shown. As expected, the response amplitude increases as the excitation amplitude increases.

5.4. System response to base longitudinal rotational speed and acceleration

The gyroscope is used to measure the rotation rate around longitudinal axis. In Fig. 8 is shown the system output for a case in which the base has a constant rotational speed along its longitudinal axis only. It is clear that the oscillation amplitude, in the u_2 direction, increases with increased rotation rate input. It is also apparent that the excitation amplitude, in the u_3 direction, does not vary with increased base rotational speed due to constant excitation force amplitude. Note that the excitation frequency is kept unchanged at the beam resonance frequency. In most models, these secondary effects are ignored. However, as demonstrated here some of these effects can be very significant. The system response to an input with zero initial rotational speed but with a constant rotational acceleration is shown in Fig. 9.

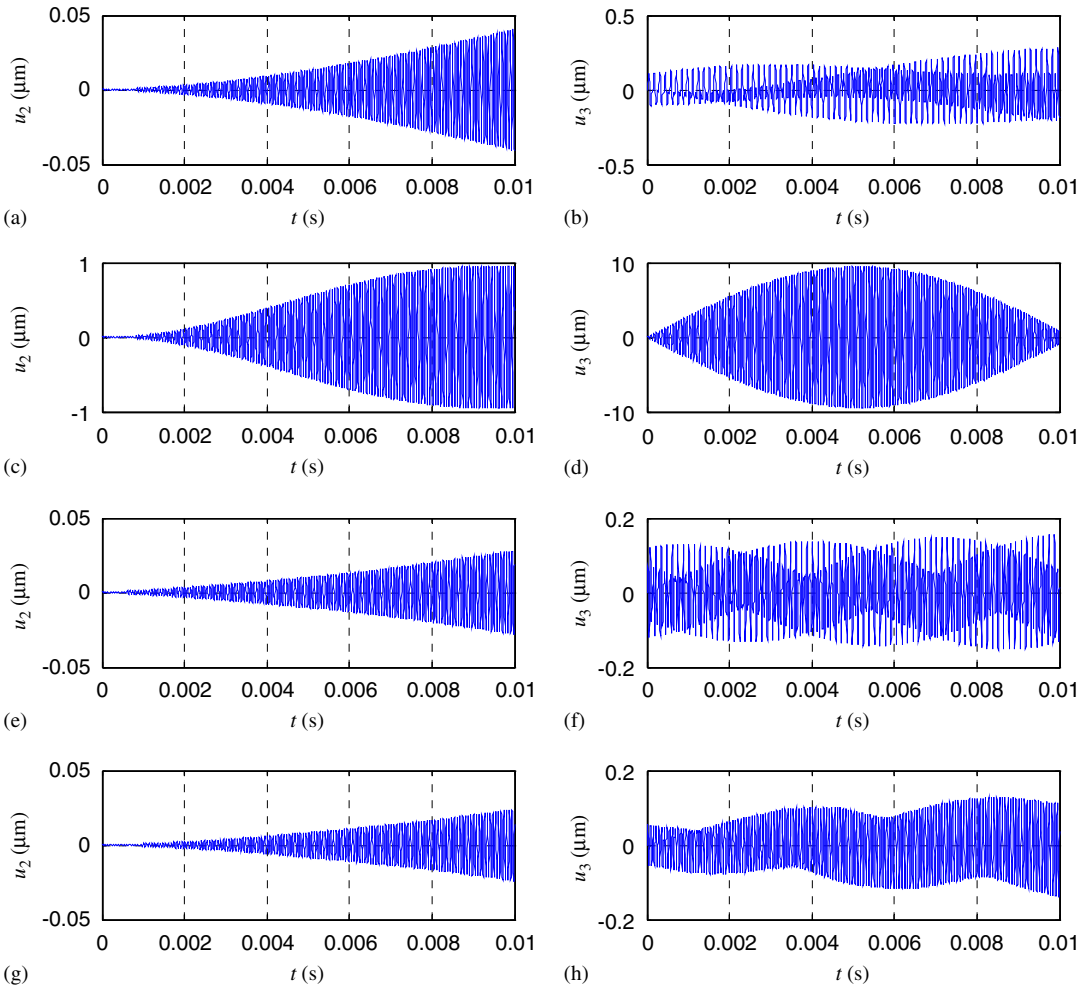

Fig. 6. The system response to different excitation frequencies (resonance frequency at $\omega_0 = 93\,601$ rad/s); sense mode: (a) $\omega_{f3} = 0.5\omega_0$, (c) $\omega_{f3} = \omega_0$, (e) $\omega_{f3} = 1.5\omega_0$, and (g) $\omega_{f3} = 2\omega_0$, drive mode: (b) $\omega_{f3} = 0.5\omega_0$, (d) $\omega_{f3} = \omega_0$, (f) $\omega_{f3} = 1.5\omega_0$ and (h) $\omega_{f3} = 2\omega_0$.

5.5. System response to linear acceleration input

The effect of linear accelerations is normally filtered out in oscillating beam gyroscopes. From results in Fig. 10 it can be seen that linear accelerations $\dot{V}_1$ and $\dot{V}_3$ do not affect the vibrations in the sensing direction but $\dot{V}_2$ is present in the response (see Fig. 11).

5.6. The cross axes effects

The cross axes effects become apparent when a combination of rotation and linear input velocities are introduced to the gyroscope. These effects show themselves in the equations as the product of the two elements. The most important of these products are $V_1 \times \omega_3$ and $V_3 \times \omega_1$. Results shown in Figs. 12 and 13 demonstrate some representative examples of these effects. In most aerospace applications, this can be a major source of measurement error and needs to be eliminated for desirable performance. On the other hand, the effect of $V_3 \times \omega_1$ as shown in Fig. 10, can be a major source of measurement error in automotive applications.

By comparing Figs. 9 and 13, it can be seen that the error due to the effect of V_3 in combination with ω_1 is obvious. This demonstrates that special care must be taken in devising correction strategies when input rotational speeds are small but longitudinal speeds are relatively appreciable.

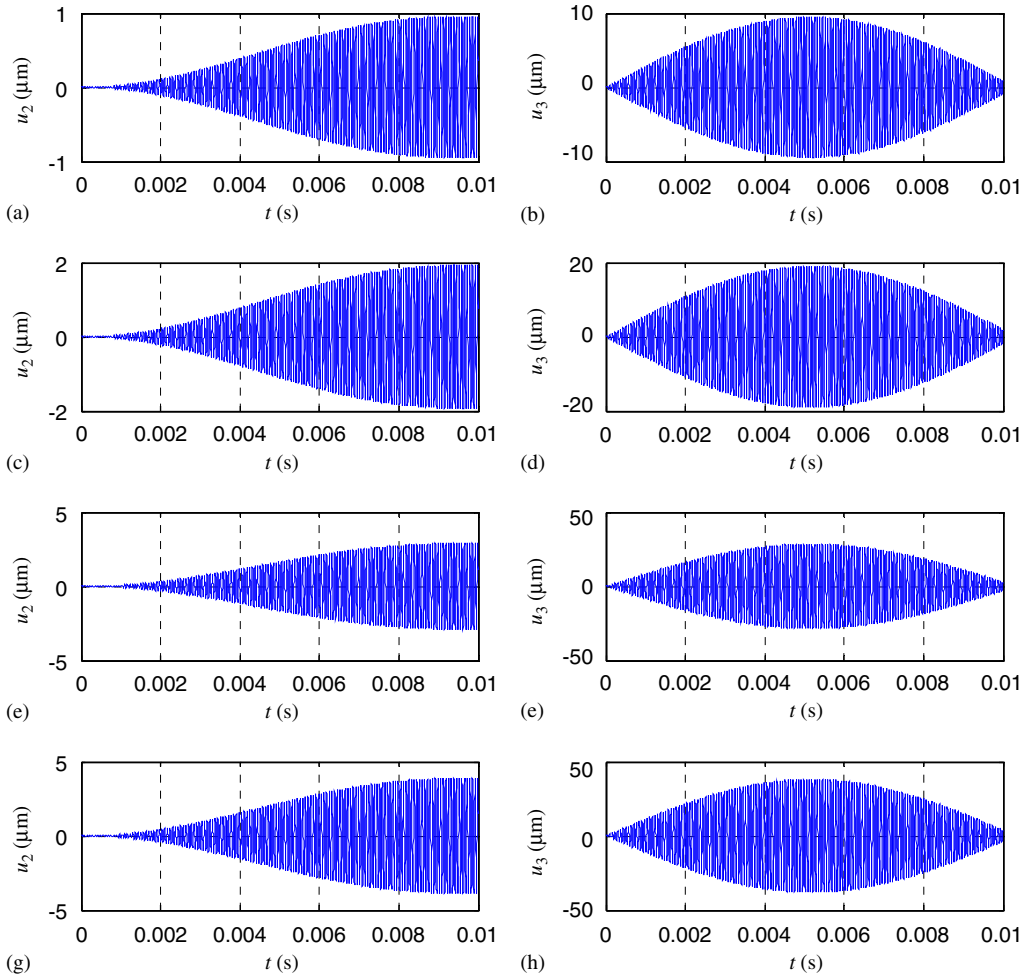

Fig. 7. The system response to excitation force amplitude. Sense mode: (a) $f_{S3} = 10$, (c) $f_{S3} = 20$, (e) $f_{S3} = 30$ and (g) $f_{S3} = 40$ nN. Drive mode: (b) $f_{S3} = 10$, (d) $f_{S3} = 20$, (f) $f_{S3} = 30$ and (h) $f_{S3} = 40$ nN.

6. Conclusions

A thorough analysis has been performed here to obtain the general equations of motion of an elastic beam with tip mass under general base excitation. The analysis was carried out further to obtain a closed-form solution for the frequency equation when the base has rotation around beam's longitudinal axis. The results were compared with those in the case of a rotating rotor with an elastic shaft. Good agreement between the current analysis for a vibrating beam having distributed and tip masses, and that of a rotor with an elastic shaft was obtained for a case in which beam base rotates along its longitudinal axis.

The effects of substrate motions on the measured output from a microgyroscope, modeled as an oscillating beam, has also been studied. The effects of changing input excitation parameters on the performance of the gyroscope have been investigated. It was concluded that an increased excitation amplitude at the resonance frequency can increase gyroscope output to input rotations. It was further concluded that major sources of error in measurements from oscillating beam gyroscopes are caused by cross axes effects resulting from a combination of lateral rotational speed and longitudinal linear speed. Therefore, special care must be taken when microgyroscope is to be used for applications with cross axes input conditions.

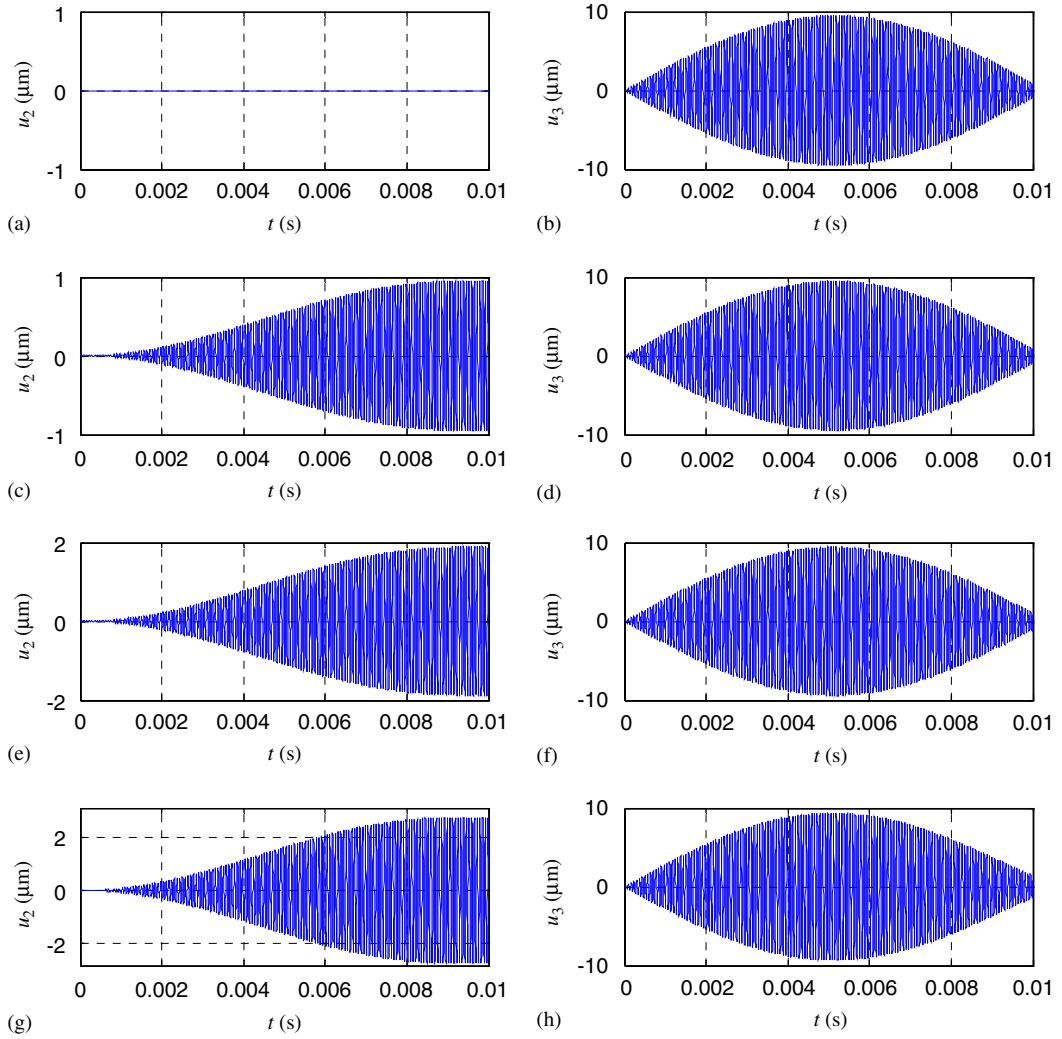

Fig. 8. System output response due to different base rotational speed. Sense mode: (a) $\omega_1 = 0$, (c) $\omega_1 = 20$, (e) $\omega_1 = 40$ and (g) $\omega_1 = 60$ rad/s. Drive mode: (b) $\omega_1 = 0$, (d) $\omega_1 = 20$, (f) $\omega_1 = 40$ and (h) $\omega_1 = 60$ rad/s.

Appendix A. Detailed derivations of the equations of motion

The Extended Hamilton's Principle for a dynamic system is widely known and is expressed as

$$\int_{t_1}^{t_2} \{\delta T - \delta V + \delta W_{nc}\}\, \mathrm{d}t = 0. \tag{A.1}$$

Utilizing the expressions for kinetic and potential energies (Eqs. (3) and (5)), different components of Eq. (A.1) can be expressed as follows.

Kinetic energy is given by

$$\begin{aligned}\int_{t_1}^{t_2} \delta T\, \mathrm{d}t &= \int_{t_1}^{t_2}\int_0^L m\delta\left(\frac{1}{2}T^*(x, u_i, V_i, \omega_i)\right)\mathrm{d}x\,\mathrm{d}t + \int_{t_1}^{t_2} M_L\delta\left(\frac{1}{2}T^*(L, u_{i_{x=L}}, V_i, \omega_i)\right)\mathrm{d}t \\ &= \int_{t_1}^{t_2}\int_0^L m(h_1\delta h_1 + h_2\delta h_2 + h_3\delta h_3)\,\mathrm{d}x\,\mathrm{d}t + \int_{t_1}^{t_2} M_L(h_1\delta h_1 + h_2\delta h_2 + h_3\delta h_3)\big|_{x=L}\,\mathrm{d}t\end{aligned}$$

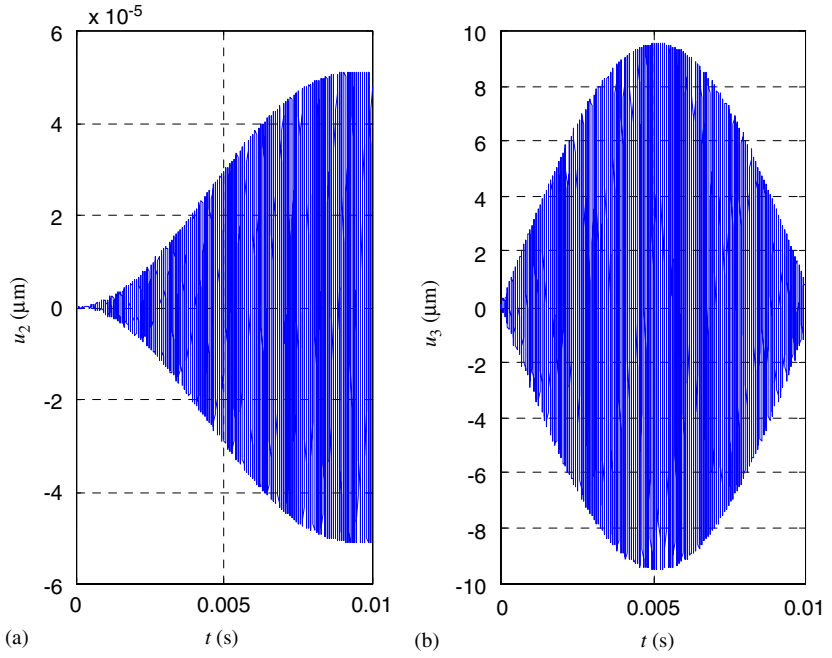

Fig. 9. System response to an input acceleration $\dot{\omega}_1 = 100\,\mathrm{rad/s^2}$: (a) sense direction and (b) drive direction.

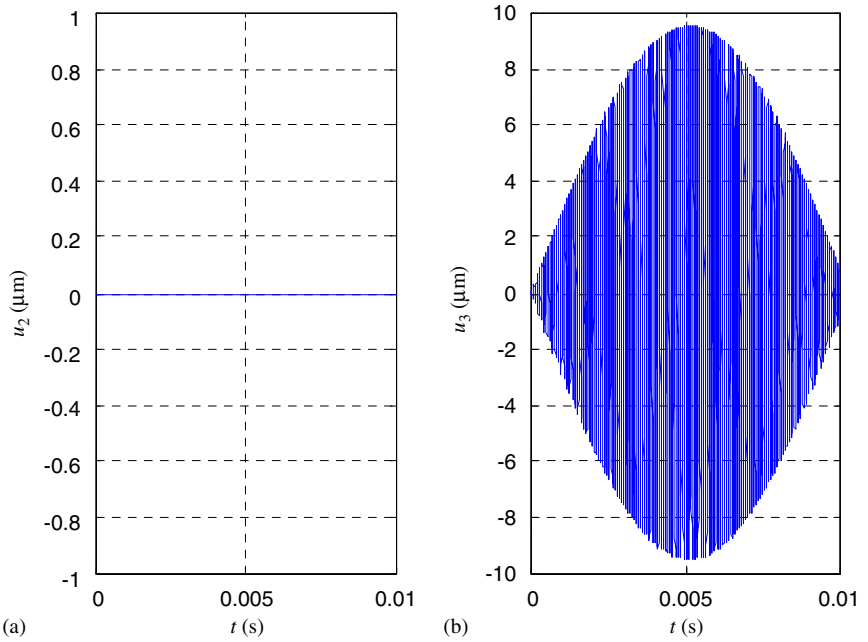

Fig. 10. The effect of linear acceleration input $\dot{V}_1$ and $\dot{V}_3 = 50\,\mathrm{m/s^2}$ on the output: (a) sense direction and (b) drive direction.

$$= \int_{t_1}^{t_2}\int_0^L m[h_1(\delta V_1 + \delta\dot{u}_1 + \delta(u_3\omega_2) - \delta(u_2\omega_3)) + h_2(\delta V_2 + \delta\dot{u}_2 + \delta(u_1\omega_3) - \delta(u_3\omega_1)$$

$$+\delta(x\omega_3)) + h_3(\delta V_3 + \delta\dot{u}_3 + \delta(u_2\omega_1) - \delta(u_1\omega_2) - \delta(x\omega_2))]\,\mathrm{d}x\,\mathrm{d}t + \int_{t_1}^{t_2} M_L[h_1(\delta V_1 + \delta\dot{u}_{1L}$$

$$+ \delta(u_{3L}\omega_2) - \delta(u_{2L}\omega)) + h_2(\delta V_2 + \delta\dot{u}_{2L} + \delta(u_{1L}\omega_3) - \delta(u_{3L}\omega_1) + \delta(L\omega_3)) + h_3(\delta V_3$$

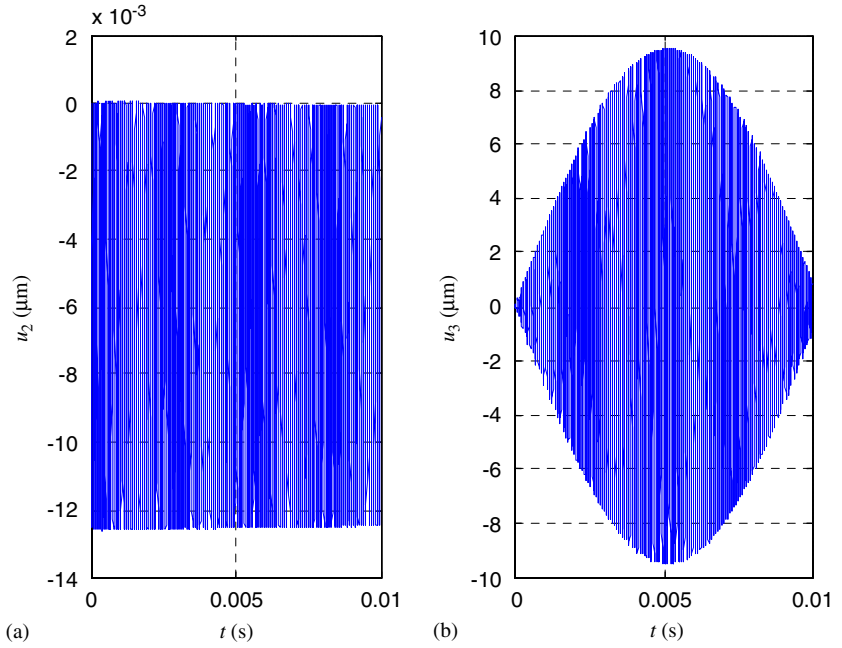

Fig. 11. The effect of linear acceleration of input $\dot{V}_2 = 50\,\mathrm{m/s^2}$ on the output: (a) sense direction and (b) drive direction.

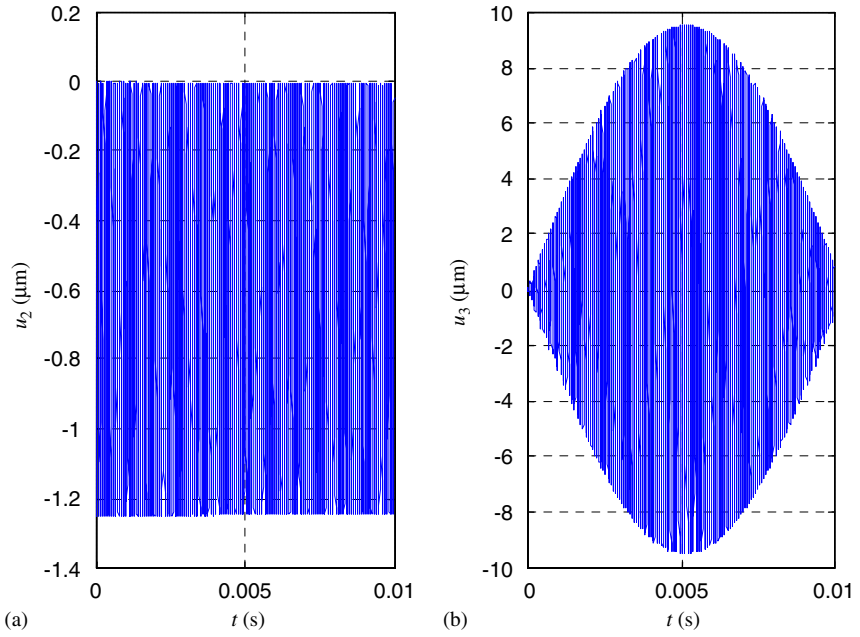

Fig. 12. Constant amplitude vibrations induced at output due to $V_1 \times \omega_3 = 5000\,\mathrm{m/s^2}$: (a) sense direction and (b) drive direction.

$$+\delta\dot{u}_{3L}+\delta(u_{2L}\omega_1)-\delta(u_{1L}\omega_2)-\delta(L\omega_2))]\,\mathrm{d}t=\int_{t_1}^{t_2}\int_0^L m\left[\left(-\frac{\partial h_1}{\partial t}+h_2\omega_3-h_3\omega_2\right)\delta u_1\right.$$
$$\left.+\left(-\frac{\partial h_2}{\partial t}-h_1\omega_3+h_3\omega_1\right)\delta u_2+\left(-\frac{\partial h_3}{\partial t}+h_1\omega_2-h_2\omega_1\right)\delta u_3\right]\mathrm{d}x\,\mathrm{d}t$$

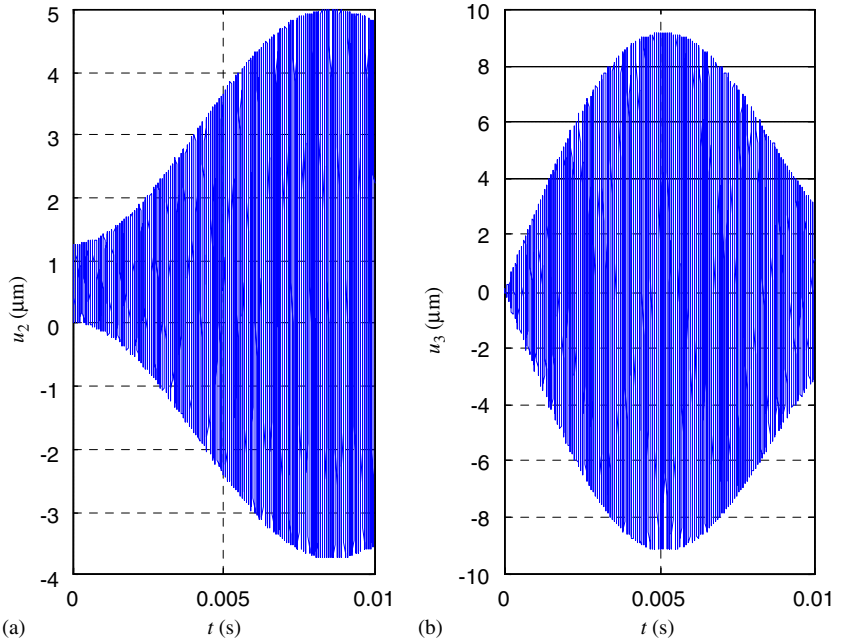

Fig. 13. Induced output oscillations due to $V_3 \times \omega_1 = 5000\,\mathrm{m/s^2}$: (a) sense direction and (b) drive direction.

$$+\int_{t_1}^{t_2} M_L\left[\left(-\frac{\partial h_1}{\partial t}+h_2\omega_3-h_3\omega_2\right)_{x=L}\delta u_{1L}+\left(-\frac{\partial h_2}{\partial t}-h_1\omega_3+h_3\omega_1\right)_{x=L}\delta u_{2L}\right.$$
$$\left.+\left(-\frac{\partial h_3}{\partial t}+h_1\omega_2-h_2\omega_1\right)_{x=L}\delta u_{3L}\right]\mathrm{d}t \tag{A.2}$$

where $u_{iL} = u_i(L,t)$.

Potential energy is given by

$$\begin{aligned}\int_{t_1}^{t_2}\delta V\,\mathrm{d}t &= \int_{t_1}^{t_2}\delta\left(\frac{1}{2}\int_0^L EA\left(\frac{\partial u_1}{\partial x}\right)^2\mathrm{d}x+\frac{1}{2}\int_0^L EI_{33}\left(\frac{\partial^2 u_2}{\partial^2 x}\right)^2\mathrm{d}x+\frac{1}{2}\int_0^L EI_{22}\left(\frac{\partial^2 u_3}{\partial^2 x}\right)^2\mathrm{d}x\right)\mathrm{d}t\\ &= \int_{t_1}^{t_2}\left[\int_0^L EA\delta\left(\frac{\partial u_1}{\partial x}\right)\frac{\partial u_1}{\partial x}\,\mathrm{d}x+\int_0^L EI_{33}\delta\left(\frac{\partial^2 u_2}{\partial^2 x}\right)\frac{\partial^2 u_2}{\partial^2 x}\,\mathrm{d}x+\int_0^L EI_{22}\delta\left(\frac{\partial^2 u_3}{\partial^2 x}\right)\frac{\partial^2 u_3}{\partial^2 x}\,\mathrm{d}x\right]\mathrm{d}t\\ &= \int_{t_1}^{t_2}\left[-\int_0^L\frac{\partial}{\partial x}\left(EA\frac{\partial u_1}{\partial x}\right)\delta u_1\,\mathrm{d}x+EA\frac{\partial u_1}{\partial x}\bigg|_{x=L}\delta u_{1L}+\int_0^L\frac{\partial^2}{\partial^2 x}\left(EI_{33}\frac{\partial^2 u_2}{\partial^2 x}\right)\delta u_2\,\mathrm{d}x\right.\\ &\quad-\frac{\partial}{\partial x}\left(EI_{33}\frac{\partial^2 u_2}{\partial^2 x}\right)\bigg|_{x=L}\delta u_{2L}+EI_{33}\frac{\partial^2 u_2}{\partial^2 x}\bigg|_{x=L}\frac{\partial}{\partial x}(\delta u_{2L})+\int_0^L\frac{\partial^2}{\partial^2 x}\left(EI_{22}\frac{\partial^2 u_3}{\partial^2 x}\right)\delta u_3\,\mathrm{d}x\\ &\quad\left.-\frac{\partial}{\partial x}\left(EI_{22}\frac{\partial^2 u_3}{\partial^2 x}\right)\bigg|_{x=L}\delta u_{3L}+EI_{22}\frac{\partial^2 u_3}{\partial^2 x}\bigg|_{x=L}\frac{\partial}{\partial x}(\delta u_{3L})\right]\mathrm{d}t\end{aligned} \tag{A.3}$$

and finally the virtual work of non-conservative forces are given by

$$\delta W_{nc} = f_{e_2}\delta u_{2L}+f_{e_3}\delta u_{3L}, \tag{A.4}$$

where f_{e_2} and f_{e_3} are applied electrostatic forces at the end of the beam in directions a_2 and a_3, respectively.

By using Eqs. (A.2)–(A.4) and taking into account the fact that variations δu_{1L}, δu_{2L}, δu_{3L}, $(\partial/\partial s)\delta u_{1L}$, $(\partial/\partial s)\delta u_{2L}$, $(\partial/\partial s)\delta u_{3L}$ and δu_1, δu_2, δu_3, δu_{1L} could have any arbitrary values; the coefficients of these expressions in Hamilton's equation must vanish. Consequently, the system governing equations along with the boundary conditions (at the tip) are as given in Eq. (6) in the main body of the paper.

Appendix B. Detailed derivations of frequency equation

Taking the temporal and spatial Laplace transformations of Eq. (9) in terms of Laplace parameters s and p yields

$$\begin{aligned}
&p^4\bar{u}_2(p,s)+k_1s^2\bar{u}_2(p,s)-k_2s\bar{u}_3(p,s)-p^3\bar{u}_2(0,s),\\
&-p^2\bar{u}_2'(0,s)-p\bar{u}_2''(0,s)-\bar{u}_2'''(0,s)=0,\\
&p^4\bar{u}_3(p,s)+k_1s^2\bar{u}_3(p,s)+k_2s\bar{u}_2(p,s)-p^3\bar{u}_3(0,s),\\
&-p^2\bar{u}_3'(0,s)-p\bar{u}_3''(0,s)-\bar{u}_3'''(0,s)=0,
\end{aligned} \tag{B.1}$$

where notations $\bar{u}_2'(0,s)=(\partial\bar{u}_2(x,s))/\partial x\big|_{x=0}$, $\bar{u}_2''(0,s)=(\partial^2\bar{u}_2(x,s))/\partial x^2\big|_{x=0}$, …, have been utilized in Eq. (B.1) for a more compact representation of the equations. If the beam support is assumed to be fixed in the moving coordinate system $\{\mathbf{a}_i\}$, then taking the temporal Laplace yields

$$\bar{u}_2(0,s)=0,\ \bar{u}_2'(0,s)=0,\ \bar{u}_3(0,s)=0,\ \bar{u}_3'(0,s)=0. \tag{B.2}$$

Substituting Eq. (B.2) into Eq. (B.1) and further simplifications yields:

$$\begin{aligned}
\bar{u}_2(p,s)&=\frac{k_2sA+(p^4+k_1s^2)B}{(p^4+k_1s^2)^2+k_2^2s^2},\\
\bar{u}_3(p,s)&=\frac{(p^4+k_1s^2)A-k_2sB}{(p^4+k_1s^2)^2+k_2^2s^2},\\
A&=p\bar{u}_3''(0,s)+\bar{u}_3'''(0,s),\ B=p\bar{u}_2''(0,s)+\bar{u}_2'''(0,s),
\end{aligned} \tag{B.3}$$

where $\bar{u}_3''(0,s)$, $\bar{u}_3'''(0,s)$, $\bar{u}_2'''(0,s)$ and $\bar{u}_2''(0,s)$ are yet to be determined. Taking the inverse spatial Laplace transformation of Eq. (B.3) will result in

$$\begin{aligned}
\bar{u}_2(x,s)&=k_2s\big(f_1'\bar{u}_3''(0,s)+f_1\bar{u}_3'''(0,s)\big)+\big(f_2'\bar{u}_2''(0,s)+f_2\bar{u}_2'''(0,s)\big),\\
\bar{u}_3(x,s)&=\big(f_2'\bar{u}_3''(0,s)+f_2\bar{u}_3'''(0,s)\big)-k_2s\big(f_1'\bar{u}_2''(0,s)+f_1\bar{u}_2'''(0,s)\big),\\
f_1(x,s)&=\underset{p}{\Im}^{-1}\left(\frac{1}{(p^4+k_1s^2)^2+k_2^2s^2}\right),\\
f_2(x,s)&=\underset{p}{\Im}^{-1}\left(\frac{p^4+k_1s^2}{(p^4+k_1s^2)^2+k_2^2s^2}\right).
\end{aligned} \tag{B.4}$$

Taking the temporal Laplace transformation of the boundary conditions given in Eq. (9) with zero initial conditions will also yield:

$$\begin{aligned}
&\bar{u}_2'''(L,s)-rLk_1s^2\bar{u}_2(L,s)+rLk_2s\bar{u}_3(L,s)=0,\\
&\bar{u}_2''(L,s)=0,\\
&\bar{u}_3'''(L,s)-rLk_1s^2\bar{u}_3(L,t)-rLk_2s\bar{u}_2(L,s)=0,\\
&\bar{u}_3''(L,s)=0.
\end{aligned} \tag{B.5}$$

Substituting expressions (B.4) into Eq. (B.5) will result in a system of four homogenous equations in terms of $u_3''(0,s)$, $u_3'''(0,s)$, $u_2'''(0,s)$ and $u_2''(0,s)$:

$$\begin{bmatrix} f_2'''' & f_2''''' - rLk_1s^2f_2' - rLk_2^2s^2f_1' & -k_2sf_1'''' & k_2s(-f_1''''' + rLk_1s^2f_1' - rLf_2') \\ f_2'' & f_2''' - rLk_1s^2f_2 - rLk_2^2s^2f_1 & -k_2sf_1'' & k_2s(-f_1''' + rLk_1s^2f_1 - rLf_2) \\ k_2sf_1'''' & k_2s(f_1''''' - rLk_1s^2f_1' + rLf_2') & f_2'''' & f_2''''' - rLk_1s^2f_2' - rLk_2^2s^2f_1' \\ k_2sf_1'' & k_2s(f_1''' - rLk_1s^2f_1 + rLf_2) & f_2'' & f_2''' - rLk_1s^2f_2 - rLk_2^2s^2f_1 \end{bmatrix}^{\mathrm{T}} \begin{bmatrix} \bar{u}_2''(0,s) \\ \bar{u}_2'''(0,s) \\ \bar{u}_3''(0,s) \\ \bar{u}_3'''(0,s) \end{bmatrix} = \begin{bmatrix} 0 \\ 0 \\ 0 \\ 0 \end{bmatrix}. \quad \text{(B.6)}$$

To obtain a non-trivial solution for the unknowns in Eq. (B.6), the determinant of the coefficients matrix must vanish. Moreover, the determinant of the coefficients is actually the denominator of the transfer function obtained from the temporal Laplace transformation. Hence, some values can be found for "s" that makes the determinant equal to zero. The imaginary part of the roots of this equation is actually the principle mode frequencies of the system. The determinant of the coefficients is given by

$$\begin{aligned} Det = {} & (r\gamma^4 \sin\beta \cosh\beta + r\lambda^4 \mathrm{i} \sin\beta \cosh\beta - r\gamma^4 \sinh\beta \cos\beta - r\lambda^4 \mathrm{i} \sinh\beta \cos\beta \\ & + \beta^3 \cosh\beta \cos\beta + \beta^3)(r\gamma^4 \sin\alpha \cosh\alpha - r\lambda^4 \mathrm{i} \sin\alpha \cosh\alpha - r\gamma^4 \sinh\alpha \cos\alpha \\ & + r\lambda^4 \mathrm{i} \sinh\alpha \cos\alpha + \alpha^3 \cosh\alpha \cos\alpha + \alpha^3), \end{aligned} \quad \text{(B.7)}$$

where

$$\begin{aligned} & \alpha^4 = -\gamma^4 + \lambda^4 \mathrm{i},\ \beta^4 = -\gamma^4 - \lambda^4 \mathrm{i}, \quad \mathrm{i} = \sqrt{-1}, \\ & \gamma^4 = k_1 s^2, \quad \lambda^4 = k_2 s, \quad r = \frac{M_L}{mL}, \quad k_1 = \frac{m}{EI}, \quad \text{and} \quad k_2 = \frac{2\omega_1 m}{EI}. \end{aligned} \quad \text{(B.8)}$$

Equating Eq. (B.7) to zero, the characteristic equation of the system in terms of s can be obtained in which the imaginary part of the roots will result in the frequencies. Eq. (B.7) can then be simplified as given by Eq. (10) in the text.

References

[1] R. Bhat, H. Wagner, Natural frequencies of a uniform cantilever with a tip mass slender in the axial direction, *Journal of Sound and Vibration* 45 (1976) 304–307.

[2] G.L. Anderson, Natural frequencies of a cantilever with an asymmetrically attached tip mass, *AIAA Journal* 16 (1978) 281–282.

[3] L.A. Parnell, M.H. Cobble, Lateral displacement of a vibrating cantilever with a concentrated mass, *Journal of Sound and Vibration* 44 (1976) 499–511.

[4] P.A.A. Laura, J.L. Pombo, E.A. Susemihl, A note on the vibrations of a clamped-free beam with a mass at the free end, *Journal of Sound and Vibration* 37 (1974) 161–168.

[5] M. Gürgöze, On the eigenfrequencies of a cantilever beam with attached tip mass and a spring mass system, *Journal of Sound and Vibration* 190 (1996) 149–162.

[6] J.Y.L. Ho, Direct path method for flexible multibody spacecraft dynamics, *Journal of Spacecraft and Rockets* 14 (1977) 102–110.

[7] C.S. Bodley, A.D. Devers, A.C. Park, H.P. Frisch, A digital computer for dynamic interaction simulation of controls and structure (DISCOS), NASA Technical Paper, 1978, p. 1219.

[8] N. Barbour, G. Schmidt, Inertial sensor technology trends, *IEEE Sensors Journal* 1 (2001) 332–339.

[9] N. Yazdi, F. Ayazi, K. Najafi, Micro-machined inertial sensors, *Proceedings of IEEE* 86 (1998) 1640–1658.

[10] A. Shkel, R. Horowitz, A. Seshia, S. Park, R.T. Howe, Dynamics and control of micro-machined gyroscopes, *American Control Conference*, San Diego, CA, USA, 1999, pp. 2119–2124.

[11] A. Shekel, R.T. Howe, R. Horowitz, Modeling and simulation of micromachined gyroscopes in the presence of imperfections, *International Conference on Modeling and Simulation of Microsystems*, San Juan, Puerto Rico, 1999, pp. 605–608.

[12] S. Park, R. Horowitz, Adaptive control for z-axis MEMS gyroscopes, *American Control Conference*, Arlington, VA, USA, 2001, pp. 496–501.

[13] W.A. Clark, Micromachined Vibratory Rate Gyroscope, PhD Dissertation, University of California, Berkeley, 1994.

[14] W.O. Davis, Mechanical Analysis of Vibratory Micromachined Gyroscopes, PhD Dissertation, University of California, Berkeley, 2001.

[15] S.D. Park, W.K. Chung, Y. Youm, J.W. Lee, Analysis of the motion of a cart with an inverted flexible beam and a concentrated tip mass, *Proceedings of Korean Automatic Control Conference (KACC)*, Pusan, Korea, 1998, 367–372.
[16] E.H.K. Fung, Z.X. Shi, Vibration frequencies of a constrained flexible arm carrying an end mass, *Journal of Sound and Vibration* 204 (1997) 259–269.
[17] W.H. Liu, C. Huang, Free vibration of a restrained beam carrying concentrated masses, *Journal of Sound and Vibration* 123 (1988) 31–42.
[18] N.G. Stephen, Note on the combined use of Dunkerley's and Southwell's method, *Journal of Sound and Vibration* 83 (1982) 585–587.
[19] S. Park, W.K. Chung, Y. Youm, J.W. Lee, Natural frequencies and open-loop responses of an elastic beam fixed on a moving cart and carrying an intermediate lumped mass, *Journal of Sound and Vibration* 230 (2000) 591–615.
[20] M. Gürgöze, Comments on a technical note by C.A. Rossi and P.A.A. Laura, *Ocean Engineering* 29 (2002) 299–302.